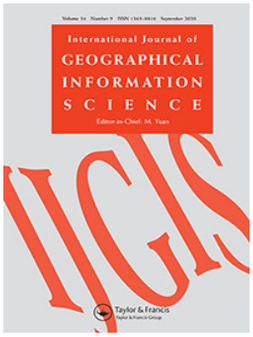

International Journal of Geographical Information Science

ISSN: (Print) (Online) Journal homepage: https://www.tandfonline.com/loi/tgis20

A spatio-temporal method for crime prediction using historical crime data and transitional zones identified from nightlight imagery

Bo Yang , Lin Liu , Minxuan Lan , Zengli Wang , Hanlin Zhou & Hongjie Yu

To cite this article: Bo Yang , Lin Liu , Minxuan Lan , Zengli Wang , Hanlin Zhou & Hongjie Yu (2020) A spatio-temporal method for crime prediction using historical crime data and transitional zones identified from nightlight imagery, International Journal of Geographical Information Science, 34:9, 1740-1764, DOI: 10.1080/13658816.2020.1737701

To link to this article: https://doi.org/10.1080/13658816.2020.1737701

INTERNATIONAL JOURNAL OF GEOGRAPHICAL INFORMATION SCIENCE
2020, VOL. 34, NO. 9, 1740–1764
https://doi.org/10.1080/13658816.2020.1737701

Taylor & Francis
Taylor & Francis Group

RESEARCH ARTICLE

A spatio-temporal method for crime prediction using historical crime data and transitional zones identified from nightlight imagery

Bo Yang [a,b], Lin Liu [b], Minxuan Lan [b], Zengli Wang [b,c], Hanlin Zhou [b] and Hongjie Yu [d]

[a]Department of Sociology, University of Central Florida, Orlando, FL, USA; [b]Department of Geography and GIS, University of Cincinnati, Cincinnati, OH, USA; [c]College of Civil Engineering, Nanjing Forestry University, Nanjing, China; [d]Center of Integrated Geographic Information Analysis, School of Geography and Planning, Sun Yat-Sen University, Guangzhou, China

ABSTRACT

Accurate crime prediction can help allocate police resources for crime reduction and prevention. There are two popular approaches to predict criminal activities: one is based on historical crime, and the other is based on environmental variables correlated with criminal patterns. Previous research on geo-statistical modeling mainly considered one type of data in space-time domain, and few sought to blend multi-source data. In this research, we proposed a spatio-temporal Cokriging algorithm to integrate historical crime data and urban transitional zones for more accurate crime prediction. Time-series historical crime data were used as the primary variable, while urban transitional zones identified from the VIIRS nightlight imagery were used as the secondary co-variable. The algorithm has been applied to predict weekly-based street crime and hotspots in Cincinnati, Ohio. Statistical tests and Predictive Accuracy Index (PAI) and Predictive Efficiency Index (PEI) tests were used to validate predictions in comparison with those of the control group without using the co-variable. The validation results demonstrate that the proposed algorithm with historical crime data and urban transitional zones increased the correlation coefficient by 5.4% for weekdays and by 12.3% for weekends in statistical tests, and gained higher hit rates measured by PAI/PEI in the hotspots test.

ARTICLE HISTORY
Received 16 September 2019
Accepted 28 February 2020

KEYWORDS
Crime prediction; spatio-temporal modeling; Cokriging; VIIRS nightlight

1. Introduction

There is a tremendous growth in the collection of spatio-temporal data about the physical and sociological processes of interest. The big data processing has tremendously facilitated the analysis in social sciences (Kitchin 2014) and criminology (Chan and Bennett Moses 2016). By investigating the spatio-temporal patterns that criminal activities follow, it is pivotal to gain further knowledge modeling criminal regulation. The utilization of a rigorous statistical approach to generate intelligence from big data processing is referred as prediction and forecasting. Crime predicting is a practical topic for both police agencies and academic

CONTACT Lin LIU Lin.Liu@uc.edu

researchers. Police forces worldwide have used mapping tools for many decades to visualize and model past crime patterns (Groff and La Vigne 2002). Therefore, accurate crime prediction affords tremendous advantages on the arrangements of police forces, including planning effective proactive interventions, reducing the level of crime, promoting public safety, and improving the efficiency with which resources are allocated (Ratcliffe 2016).

Numerous crime prediction methods have been developed using historical criminal activities in the region of interest. Some studies used historical data to create spatio-temporal forecasting of criminal activities allocating spatial and temporal patterns for deterring and detecting criminal activities (Ratcliffe 2016). Short *et al*. (2010) proposed a Partial Differential Equations (PDEs) reaction-diffusion model, which provided a mechanistic explanation for crime pattern given simple assumptions about the diffusion of the crime risk and localized search by offenders. Furthermore, the self-exciting point process (SEPP) model is a recently developed crime prediction method with inputs of the locations and time of historic crimes. SEPP model achieved a valid prediction result when applied to a residential burglary dataset from Los Angeles, USA (Mohler *et al*. 2011, Mohler 2014).

On the other hand, many crime prediction studies utilized the environmental variables which correlated with crime patterns. Gerber (2014) investigated the use of spatio-temporal tagged tweets for crime prediction in Chicago. There are also studies using geo-tagged Twitter data to facilitate the modeling of criminal activities (Bendler *et al*. 2014, Corso *et al*. 2016). Patino *et al*. (2014) utilized the land-use data derived from remote sensing images to investigate the influence of the land-use and urban layout on homicide, and conclusions were made that global neighborhood homogeneity was negatively related to homicide rates. Nevertheless, it only investigated the spatial relationship between land-use and homicide, which could not be applied to crime prediction over the temporal domain.

Criminal activities can be treated as a spatio-temporal process of social science, which is challenging to be incorporated with environmental variables. This entails the development of a valid spatio-temporal structure to combine the measurements from multi-source data into consideration. The fact that few studies have comprehensively incorporated both historical crime data and environmental variables underscore the theoretical and technical challenges on integrating multi-source data for advanced crime predictions. Difficulties of incorporating multi-source data come from the modeling of cross-covariance between different datasets, estimation of valid spatio-temporal structure, and justifications of the use of environment variable(s).

Studies over the past two decades have made major strides on spatial or space-time geostatistical methods. Skøien and Blöschl (2007) proposed a spatio-temporal kriging method for estimating runoff time series, and Snepvangers *et al*. (2003) presented a spatio-temporal kriging method with external drift for assimilating the soil water content. Although those studies demonstrated valid methods for analyses in a space-time domain, they adopted the ordinary/universal kriging method dealing with a single type of variable. On the other hand, Cokriging is formulated as one of the extensions of Kriging system to more than one variable in space domain: one primary target variable, and one or more secondary co-variable(s). Pardo-Igúzquiza *et al*. (2006) developed a downscaling Cokriging method for remote sensing data sharpening, in which the primary variable and the secondary covariable were both wisely considered. But downscaling Cokriging method does not model the temporal dimension. Sahoo *et al*. (2018) proposed a space-time Cokriging, which adopted multiple co-variables as latent variables in Cokriging system to predict the groundwater

level. Pravilovic *et al*. (2018) developed a Cokriging spatio-temporal interpolator ($CoST^k$) which used a window operator to consume its time-evolving data. However, the temporal structures in both studies were modeled from exploratory analysis rather than statistical approach. The spatio-temporal structure was built by sequencing months of temporal data or combining spatial dependency with temporal principal component. Those methods are rather limited in the time-sensitive sociological processes because of the lack of rigorous statistical variograms. Studies modeling the temporal statistics are often problematic from too many parameters (Wang and Brown 2012, Law *et al*. 2014).

Remote sensing nighttime imagery has been widely used for modeling urban structure (Liu *et al*. 2012, Yu *et al*. 2014, Chen *et al*. 2017), population and economic (Sutton 1997, Shi *et al*. 2014), and predicting poverty (Jean *et al*. 2016, Proville *et al*. 2017). In this study, the nightlight imagery was used to identify urban transitional zones via the edge detection technique. Previous research demonstrated that hotspots of crime often occur along the edges or transitional zones between urban neighborhoods and districts, for instance, 42nd Street in New York, or Granville Street in Vancouver (Brantingham *et al*. 1977, Brantingham and Brantingham 1995). Strangers are more acceptable because they frequently and legitimately present around transitional zones. Transitional zones may also contain mixes of land uses and physical features, which lead to crime generators and attractors (Shaw and McKay 1942, Suttles 1968, Herbert and Hyde 1985, Brantingham and Brantingham 1995). To enhance the street crime prediction, transitional zones were utilized as an environmental variable in the ST-Cokriging algorithm as the co-variable for an application example of the City of Cincinnati in 2012. This research extended traditional Cokriging from a spatial domain to a space-time domain, and proposed a spatio-temporal Cokriging (ST-Cokriging) technique for crime prediction. The primary variable determines the overall trend of predicted values while the secondary co-variable exerts the local spatial pattern. We derived a spatio-temporal structure taking into account the spatial and temporal covariances and cross-covariance within and between two types of source data. This is the first attempt of incorporating transitional zones into a statistical spatio-temporal model that synergistically integrates multi-source data for crime prediction. In this research, crime data were further processed to continuous crime risk maps and aggregated to weekday and weekend groups. The ST-Cokriging algorithm was used to generate predictive crime risk maps and crime hotspots maps. The validation and accuracy assessments demonstrated that the utilization of transitional zones as the secondary co-variable successfully enhanced the crime-predicting performance. It yielded higher correlation value and higher hit rate when validating against the actual references crime data.

2. Study area and data

2.1. Study area and crime data

The City of Cincinnati (hereafter Cincinnati) locates in the south of Ohio. It is the third largest city in the state with a population of 298,550 people and 166 constituent neighborhoods as in 2010. A lot of the housing stock was built prior to World War II, which makes it one of the most historic cities in the country.

Started from early 2006, the Cincinnati Police Department initiated 'Operation Vortex' – an aggressive patrol unit designed to reduce crime through high numbers of arrests. The

initial police report of the success of the program touted falling crime rates in the Over-the-Rhine (OTR) neighborhood and stressed the importance and value of the patrol unit. Based on its successes in OTR, later the city decided to make the Vortex Unit a permanent feature of the Cincinnati Police (Hall and Liu 2009). Crime rates in Cincinnati have dropped in all categories from 2006 to 2010. However, according to the FBI's report, Cincinnati still ranked as the 16th most dangerous city in the United States in 2010. Since the high crime rates have been a long-term problem, the precise crime prediction could help the police department to better arrange the police force and substantially reduce crime rates.

Figure 1 shows the spatial distributions of all robberies and assaults in Cincinnati in 2012. The crime data were acquired from the Cincinnati Police Department. These crime records contain the crime type, reported time, location, geographical coordinates, etc. In this research, we aimed to predict the crime with the input of historical crime data and transitional zones. The target crime type was set to street crime because transitional zones of the streets, business centers, and industry distributions are spatially correlated with the street crime (Welsh and Farrington 2002). Robberies and assaults are selected from all crime types as the target criminal type. Other crime types such as burglary and domestic violence are not included in this research.

2.2. Acquisition of nightlight remote sensing data

We acquired the monthly Visible Infrared Imaging Radiometer Suite (VIIRS) nightlight images from The Earth Observations Group (EOG) at NOAA/NGDC (ngdc.noaa.gov). The

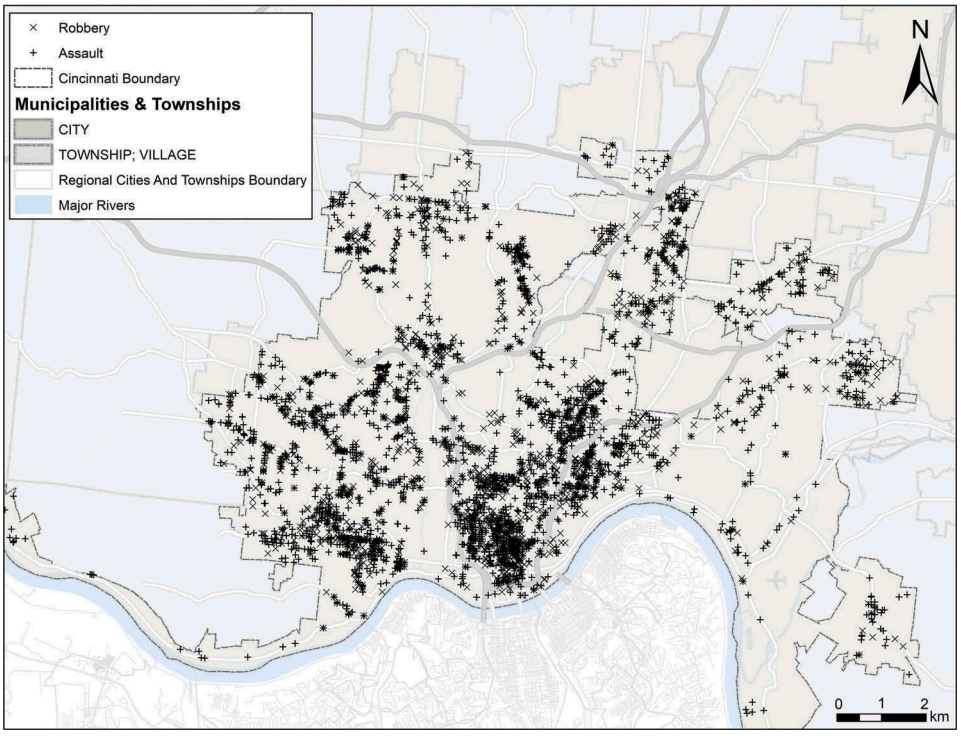

Figure 1. Robbery and assault distributions overlay with city map in Cincinnati in 2012.

VIIRS night light data were processed for a monthly based temporal average value. We cropped the VIIRS nightlight images to the spatial extent of Cincinnati and projected to the NAD 1983 State Plane Ohio South coordinate system. Afterward, a three-by-three Gaussian filter with a sigma of 1 was performed on nightlight imagery to filter out lights from aurora, fires, boats, and other temporal lights (Chen *et al*. 2015, 2017).

Because of the blocking effect of vegetation canopy, VIIRS nightlight imagery shows a relatively higher radiance in the winter months (Li *et al*. 2017, Zhao *et al*. 2017). As shown in Figure 2, the nightlight image of Cincinnati has been adjusted to the same color representations. Apparently, the image in December (Figure 2(a)) shows higher radiance and contrast than in August (Figure 2(b)). Therefore, the nightlight image in December is used to extract the transitional zones because it is clearer to represent the distribution of streets, industries, and business centers.

2.3. Edge detection on nightlight imagery

Numerous edge detectors were developed for modeling the urban structure from the remote sensing imagery. They are typically classified in two broad classes, gradient operators and second derivative operators (Ali and Clausi 2001, Kaur and Garg 2011). Gradient operators respond with a broad peak at an edge location, thus require a thinning or maximum detection step (Binford 1981). In this research, the advanced Laplacian of Gaussian (LoG) filter was used as the edge detector for VIIRS nightlight imagery (Figure 3(a)). The filter performs as an application of a smoothing filter followed by a derivative (Canny 1986, Maini and Aggarwal 2009). Regions with multiple histogram peaks were selected to represent the pixel distribution as a function of tonal variation. By modeling the histogram, it is feasible to judge the entire tonal distribution; therefore, the histogram can be analyzed for peaks or valleys which can be used to determine threshold values (Sarkar and Basu 2014). A 5 $\times$ 5 convolution kernel is selected for extracting transitional zones. The LoG filter normally takes a single grey level image as input and produces another grey level image as output. The transitional zone generated in this study is a single band continuous raster map which highlights regions of rapid intensity changes.

In the edge detection map (Figure 3(a)), the downtown area next to the Ohio River remains solid hotspots zone, while edge zones in suburban areas in the north of downtown are depicted in ring shapes. Liu and Wang (2016) estimated the polycentric urban

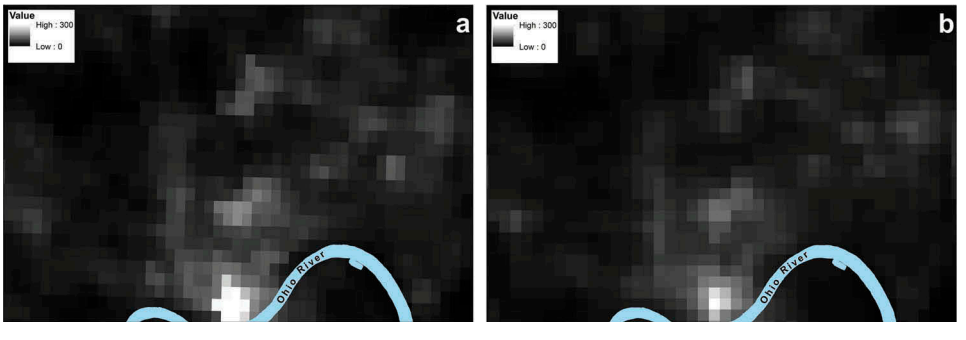

Figure 2. VIIRS nightlight images for Cincinnati in: (a) December of 2012; (b) August of 2012.

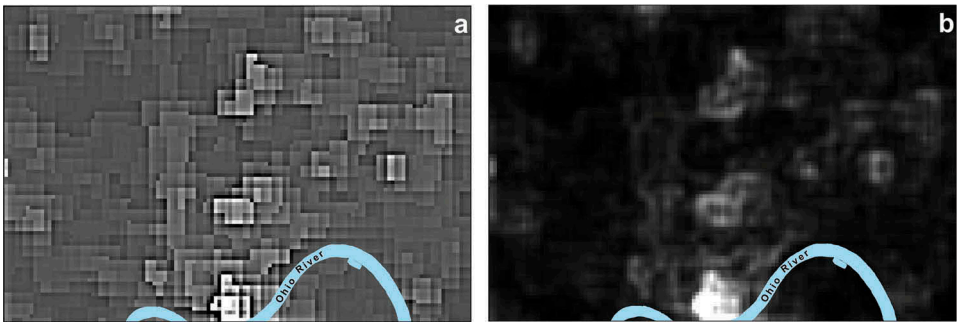

Figure 3. (a): VIIRS LoG edge detection result; (b): processed the transitional zone map of Cincinnati.

structure by identifying multiple subcenters and emphasizing the rising importance of suburban centers and the dynamic linkages among the downtown area, suburban centers, and transitional zones of metropolitan areas. Following the study that estimate the urban spatial structure from the nighttime light imagery (Chen *et al*. 2017), we calculated the minimum distance between the main center (downtown) and subcenters that gradually developed from small suburb towns, so that the transitional zones from different centers were able to be well extracted without being mixed. The minimum distance between subcenters is about 1.6 km, so an 800-m gradient buffer zone was created based on the edge detection result to generate a map of urban transitional zones (Figure 3(b)).

Besides the edge detector, other methods such as Spatial Stratified Heterogeneity (SSH) can be used for extracting transitional zones (Wang *et al*. 2012). K-means grouping and regression trees are typically used to extract spatial stratification of heterogeneity or classification. SSH extracts a classification such as a belt between strata, thus is more suitable for extract transitional zone in a large area, e.g. at country level (Wang *et al*. 2016). Nonetheless, the LoG filter is best suited for detecting transitional zones in this study.

3. Methodology

3.1. Mathematical formulation of ST-Cokriging

In geo-statistics, Cokriging is formulated as one of the extensions of the Kriging system to more than one variable in the space domain. Taking into account the spatial correlation between the primary target variable and secondary co-variable(s), Cokriging can provide a more accurate prediction of the target variable than ordinary or universal Kriging (Cressie 1993, Chilès and Delfiner 1999). Transitional zones as the secondary variable in this study have more density measurements in the spatial domain than the point-like criminal activities, hence are suitable to be used to enhance the crime prediction as the co-variable.

The proposed ST-Cokriging method accounts for both spatial and temporal correlations within and between primary and secondary variables. The primary variable stands for the street crime risk maps at time points t_{1i}, $i = 1, \ldots, T.$, and the secondary variable stands for the transitional zones at time point t_2. The ST-Cokriging prediction of the primary variable can be expressed as

$$\hat{Z}_1(x_0, t_0) = \sum_{i=1}^{T} \sum_{j=1}^{N_i} a_{ij} Z_1(s_{ij}, t_{1i}) + \sum_{k=1}^{M} \beta_k Z_2(u_k, t_2) \tag{1}$$

where $\hat{Z}_1(x_0, t_0)$ is the predictor at pixel location x_0 and at time t_0; The time point t_0 is the predicting time point which can be flexible in the temporal domain. $Z_1(s_{ij}, t_{1i})$ denotes the primary variable at location s_{ij} at time $t_{1i}, j = 1, \ldots, N_i, i = 1, \ldots, T$; $Z_2(u_k, t_2)$ denotes the secondary co-variable at location u_k at time t_2 and. $k = 1, \ldots, M$. Two sets of weights $\{a_{ij} : j = 1, \ldots, N_i; i = 1, \ldots, T\}$ and $\{\beta_k : k = 1, \ldots, M\}$ were obtained in the best linear unbiased predictor.

$$C\lambda = B \tag{2}$$

where

$$C = \begin{bmatrix} C_1^{11} & C_1^{12} & & C_1^{1T} & C_{12}^{1} & 1_{N1} & 0_{N_1} \\ C_1^{21} & C_1^{22} & \cdots & C_1^{2T} & C_{12}^{2} & 1_{N2} & 0_{N_2} \\ \vdots & & & & \vdots & & \\ C_1^{T1} & C_1^{T2} & \ddots & C_1^{TT} & C_{12}^{T} & 1_{N_T} & 0_{N_T} \\ C_{21}^{1} & C_{21}^{2} & & C_{21}^{T} & C_2 & 0_M & 1_M \\ 1'_{N_1} & 1'_{N_2} & \cdots & 1'_{N_T} & 0'_M & 0 & 0 \\ 0'_{N_1} & 0'_{N_2} & & 0'_{N_T} & 1'_M & 0 & 0 \end{bmatrix} \tag{3}$$

$$B = \begin{bmatrix} C_{11}^{10}(x_0) \\ C_{11}^{20}(x_0) \\ \vdots \\ C_{11}^{T0}(x_0) \\ C_{12}^{0}(x_0) \\ 1 \\ 0 \end{bmatrix} \tag{4}$$

and

$$\lambda = \begin{bmatrix} \alpha_{11} \\ \vdots \\ \alpha_{1N_1} \\ \alpha_{21} \\ \vdots \\ \alpha_{2N_2} \\ \vdots \\ \alpha_{TN_T} \\ \beta_1 \\ \vdots \\ \beta_M \\ m_1 \\ m_2 \end{bmatrix} \tag{5}$$

The elements in C are defined as: C_1^{il} is the $N_i \times N_l$ covariance matrix of the primary variable at time t_{1i}, $\{Z_1(s_{ij}, t_{1i}) : j = 1, \ldots, N_i\}$ is the primary variable at time t_{1l}, and C_2 is the $M \times M$

covariance matrix of secondary variable $\{Z_2(u_k, t_2) : k = 1, \ldots, M\}$attime$t_2$. Covariance C_1^{il} and C_2 are obtained from the pixel pairs with spatial lag s and temporal lag t between variable Z_1 and Z_2, C_{12}^i is the $N_i \times M$ cross-covariance matrix,$\{Z_1(s_{ij}, t_{1i}) : j = 1, \ldots, N_i\}$ and the secondary variable at time t_2. $\{Z_2(u_k, t_2) : k = 1, \ldots, M\}$ with $C_{21}^i = C_{12}^i$, In B, $C_{11}^{i0}(x_0)$ is the $N_i \times 1$ cross-covariance vector between primary variable $\{Z_1(s_{ij}, t_{1i}) : j = 1, \ldots, N_i\}$ at time t_{1i} and primary variable at time 0 and pixel x_0, $C_{12}^0(x_0)$ is the $M \times 1$ cross-covariance vector between the secondary variable $\{Z_2(u_k, t_2) : k = 1, \ldots, M\}$ and the primary variable. Weights of α_{ij} and β_k are under two constraints:

$$\sum_{i=1}^{T} \sum_{j=1}^{N_i} \alpha_{ij} = 1; \quad \sum_{k=1}^{M} \beta_k = 0 \tag{6}$$

Solving the Cokriging system, we obtained the weights:

$$\lambda = C^{-1}B \tag{7}$$

Besides, the uncertainty associated with the prediction is calculated by the spatio-temporal distribution of data and the below equation:

$$\sigma^2(x_0, t_0) = var(Z_1(x_0, t_0)) - \sum_{i=1}^{T} \alpha_i' C_{11}^{i0}(x_0) - \beta' C_{12}^0(x_0) + m_1 \tag{8}$$

where $Var\{.\}$ is the variance function; $\alpha_i = \{\alpha_{i1}, \ldots, \alpha_{iN_T}\}'$, $\beta = \{\beta_1, \ldots, \beta_M\}'$, m_1 is Lagrange multipliers (Webster and Oliver 2007, Atkinson *et al.* 2008).

3.2. Spatio-temporal covariance model

The spatial and temporal semi–variograms were constructed by modeling the covariance and cross-covariance within and between the primary variable and the co-variable. Spatial semi–variogram $\gamma_s(h_s)$was computed by selecting data pairs with the spatial distance h_s, then their average squared differences were calculated by the following equation:

$$\gamma_s(h_s) = \frac{1}{2N(h_s)} \sum_{i=1}^{N(h_s)} [Z(s_1, t_1) - Z(s_1 + h_s, t_1)]^2 \tag{9}$$

where $N(h_s)$ is the number of randomly chosen pairs. For example, $N(h_s) = 3000$ means 3,000 randomly chosen pairs on crime risk maps with a spatial distance h_s were used to calculate the spatial semi–variogram.

Next, the empirical temporal semi–variogram $\gamma(h_t)$ was calculated as the function of the temporal distance h_t in the unit of temporal aggregation of the crime data over the entire time period. Time-series data acquired in $h_t$period before or after the predicting time point were used in the following equation:

$$\gamma_t(h_t) = \frac{1}{2N(h_t)} \sum_{i=1}^{N(h_t)} [Z(s_1, t_1) - Z(s_1, t_1 + h_t)]^2 \tag{10}$$

where $N(h_t)$ is the number of data pairs which are located at the same location while separated by h_t period.

Spatio-temporal covariances have the property that they can be written as a product of a valid spatial covariance and a valid temporal covariance (Rodríguez-Iturbe and Mejía 1974, Cressie and Huang 1999). There are other spatio-temporal models developed and

discussed in spatial statistics, such as product–sum model using a combination of product and sum of the spatial and temporal covariance (De Cesare *et al*. 2001, De Iaco *et al*. 2001), and non-separable spatio-temporal stationary model (Cressie and Huang 1999). However, those models required to estimate a series of parameters, which are not computationally efficient in the spatio-temporal context. We build a valid spatio-temporal covariance taking account of time-series primary variable and co-variable. Valid spatial covariance model and valid temporal covariance model are readily available to be combined in product form, achieving the best balance between efficiency and effectiveness. Specifically,

$$Cov(Z(s,t), Z(s+h_s, t+h_t)) = C_s(h_s) \cdot R_t(h_t), \tag{11}$$

where C_s is the valid spatial covariance, and $R_t(\cdot)$ is the temporal correlation function.

The estimation of covariance matrix requires covariances within and cross primary variable and secondary covariable. Each item in the covariance matrix C represents a spatio-temporal covariance estimation with the input of spatial lag (h_s) and temporal lag (h_t). Specifically, with spatial lag accessed from the Euclidean distance h_s, items in sub-matrix $C_1^{T_r T_v}$ were calculated with temporal lag $(h_t = T_r - T_v)$ for primary variable. Items in sub-matrix C_2 were calculated with spatial lag (h_s) for secondary co-variable. Temporal lag $(h_t = 0)$ was used in sub-matrix C_2 because secondary co-variable is unique in temporal domain. Cross-covariance $C_{12}^{T_1 T_2}$ between the primary variable and secondary co-variable was synthetically estimated through Equation (11) with the input of th_s and h_t. Temporal lag $(h_t = T_1 - T_2)$ of cross-covariance was set to be the longest temporal lag in the temporal domain. Because the actual acquiring time of covariable is December, which is the longest temporal lag to the predicting time T_0, and the covariable is less sensitive to the temporal change. Consequently, T_2 for the secondary variable was appended to the last position of the time sequence of the primary variable. The cross-covariance is modeled such that the primary variable and secondary co-variable are in a consistent temporal dimension and that the entire covariance matrix is positive-definite. In the calculation of cross-covariance, the change-of-support is not involved in this study because both primary variable and secondary co-variable have been set to the same support size of 150 m (Pardo-Igúzquiza *et al*. 2006).

3.3. Accuracy evaluation

Statistical scores of Pearson Correlation Coefficient (PCC), Root Mean Squared Error (RMSE), Predictive Accuracy Index (PAI) and Predictive Efficiency Index (PEI) were used to validate the prediction results (Chainey *et al*. 2008, Hunt 2016). PCC represents the sample correlation coefficient between predictions and reference data. RMSE represents the differences between prediction and the actual reference data. PAI proposed by Chainey *et al*. (2008) is an index that measures the effectiveness of the prediction which captured the hot-spots of the crime data (Chainey *et al*. 2008). Mathematically,

$$PAI = \left(\frac{n}{N}\right) / \left(\frac{a}{A}\right) \tag{12}$$

where n is the number of crimes successfully predicted by the determined hotspot area, N is the total number of crimes within the predicted period, a is the area of crime hotspots,

and A is the total area of the region of interest. PAI can be considered as the hit rate against the areas where crimes are predicted to occur with respect to the size of the study area. Predicting 100% of criminal activities in 100% of the area would give a PAI value of 1. Predicting 25% of criminal activities in 50% of the study area would give a PAI value of 0.5, and predicting 80% of future crime in 40% of the area would give a PAI value of 2. Therefore, the larger the number of crimes predicted in a smaller hotspot area led to a higher PAI (Chainey *et al*. 2008).

PEI ranging from 0 to 1 is the ratio of actual PAI over the maximum PAI for a given hotspot scenario (Hunt 2016). PEI measures how well the crime prediction captures hotspots comparing to the optimal solution. Thus,

$$PEI = \frac{PAI}{PAI_{max}} \tag{13}$$

where PAI_{max} denotes the maximum value of possible PAI.

To validate the prediction results from ST-Cokriging, we used the forecast scenario of the crimes and validate against the actual data. Specifically, we input the time-series crime data$h$ (temporal distance) prior to the predicting time point t $(Z_{t-h}, Z_{t-h-1}, \ldots, Z_{t-1})$ to predict $\hat{Z}_t$, and validated $\hat{Z}_t$ against the actual crime data Z_t, then used time-series crime data $(Z_{t-h-1}, Z_{t-h-2}, \ldots, Z_t)$ to predict $\hat{Z}_{t+1}$ and validate the results against actual Z_{t+1}, and so forth. The predictions were validated quantitatively through PCC, RMSE, PAI, and PEI.

4. Results

4.1. Data aggregation

Crime data were aggregated for (half-) monthly basis in previous research (Levitt 2002, Mares 2013). However, the monthly aggregated data were not evenly distributed in the temporal domain because of the inequality of the number of days in each month. The duration differences for each month brought additional bias to the prediction model. To illustrate the difference, we plotted histograms of crime data in 2012 using both monthly and quad-weekly-based aggregation methods. For the quad-weekly aggregation, counting from the first Monday of a year, we aggregated the crime data every 4 weeks, which were approximately 13 quad-week periods per year. Figure 4 shows the crime frequency in Cincinnati in both monthly and quad-weekly aggregation methods. The horizontal axis represents the number of months from 1 to 12 and the number of quad-week periods from 1 to 13.

Apparently, the month-based crime frequency is higher in those months with 31 days as shown in Figure 4. For instance, January and March (month number 1 and 3) have significantly higher crime frequencies than February and April (Month number 2 and 4), which is different from frequency distribution shown in quad-week periods. Furthermore, as 2012 is a leap year, the bias could be larger for non-leap years with 28 days in February. The quad-week crime aggregation in Figure 4 is in accordance with the seasonal distribution of crime data in previous research (Baumer and Wright 1996, Andresen and Malleson 2013). Therefore, the weekly aggregation method is more reasonable and we divided the data in this way.

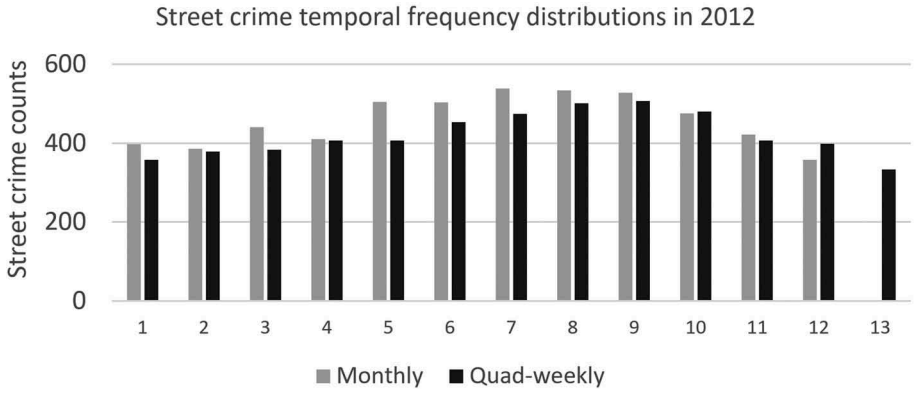

Figure 4. Monthly and quad-weekly-based street crime data aggregation in Cincinnati, 2012.

Furthermore, previous research demonstrated that the spatial pattern of crime is different between weekdays and weekends (Newton *et al*. 2008, Uittenbogaard and Ceccato 2012). As shown in Figure 5(a), crime frequencies for weekends, Sunday (day 1 in a week) and Saturday (day 7 in a week), are higher than the rest of the days in weekdays. Criminal activities in the weekends represent not only a higher frequency, but also different spatial patterns (Figure 8 in section 4.3). Hence, it is necessary to further divide crime data into two groups of weekdays and weekends. Specifically, we followed the dividing approach proposed by National *et al*. (2010). The weekend group is defined from Friday at 1800 to Sunday at 1800 local time. Weekday group is defined as the period between Sunday at 1800 and Friday at 1800 local time. The crime histogram for each day in a month was also generated (Figure 5(b)), which shows a discrete uniform distribution of crime frequency in different days of a month. Day 31 has a lower count since a month can contain anywhere from 28 to 31 days. Therefore, there is no need to separate the data by the number of day in a month.

4.2. Data pre-processing and estimation of spatio-temporal structure

The aggregated crime data in 2012 are further processed to spatial continuous crime risk maps using the kernel density function (Okabe *et al*. 2009). The output cell size of the kernel density map was set to 150 m because it is a suitable visible distance for police patrol. The primary variable has been processed weekly crime raster maps using kernel density function. The kernel density calculated the crime risk for each pixel of the map covering the study area, and transform the spatial discrete crime point to a risk map. Random variable of the crime risk pixels in the map was used as the primary variable. Therefore, the output of the crime prediction is also a continuous crime risk map. The transformation process ensured that the input crime risk normally distributed and numerically computable so that the covariance could be calculated as the covariance function evaluated at the locations of two points.

In addition, as in general kriging system, we assume the mean of each variable is constant with respect to location (and time). Therefore, a detrending process is necessary to satisfy the secondary-stationary assumption. Specifically, a trend surface imagery

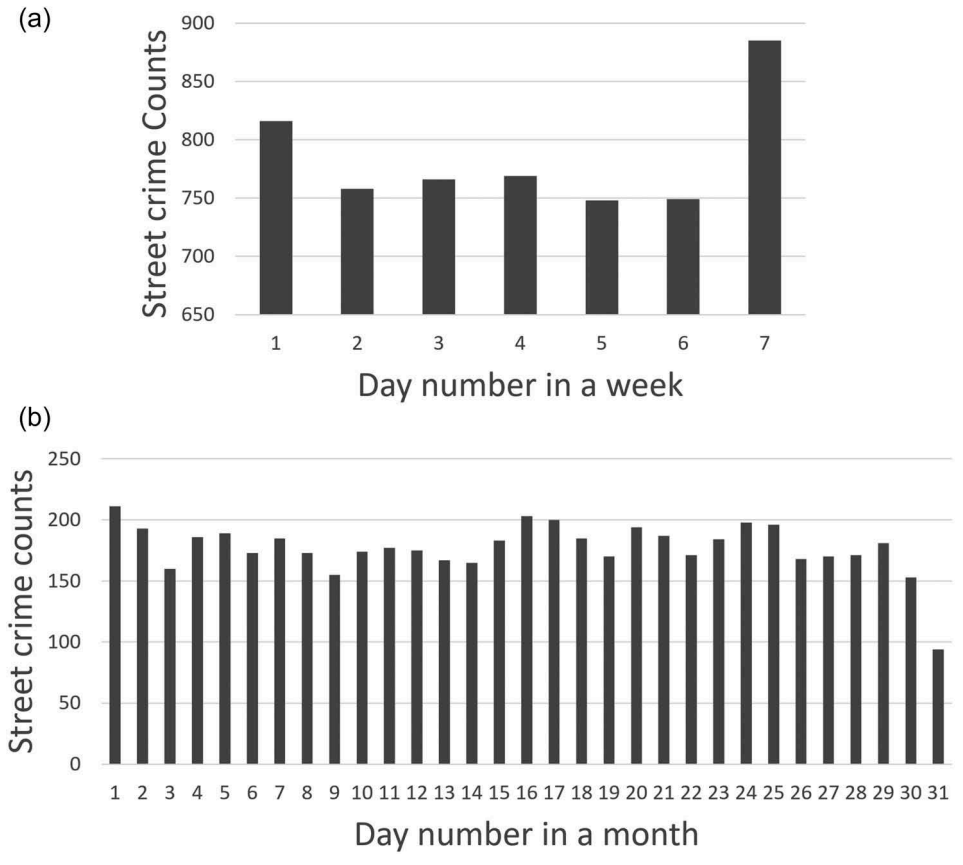

Figure 5. Street crime histogram in 2012 for: (a) difference day in a week; (b) different day in a month.

calculated from the temporal mean value of a time-series crime data was subtracted from the inputs. The residuals after removing the trend surface were used to estimate semi–variograms and correlations. The trend as deterministic surface changes gradually, while the residuals change more quickly. The large-scale variability is shaped by the trend surface, while the small-scale variability is modeled by the residual.

The spatio-temporal covariance was estimated through the calculation of empirical semi–variograms. The spatial and temporal semi–variograms were calculated based on Equation (9) and (10) using the street crime data in 2012. We selected a portion of the available street crime as the training set to estimate the semi–variograms. Once the empirical semi–variograms were obtained, the Ordinary Least Square (OLS) fitting method was used to estimate the fitting model for both spatial and temporal semi–variograms.

Figure 6 shows the empirical spatial and temporal semi–variograms for weekday group and weekend group. Apparently, shapes of semi–variograms are different for spatial and temporal domain. There are multiple fitting functions available, including linear, spherical, exponential, and Gaussian functions. Gaussian function was selected to model the spatial semi–variogram while the exponential function was selected to model the temporal semi–variogram as a result of smallest residual value from OLS fitting method, as well as the shape of the semi–variograms. This comparative model selection ensures data is

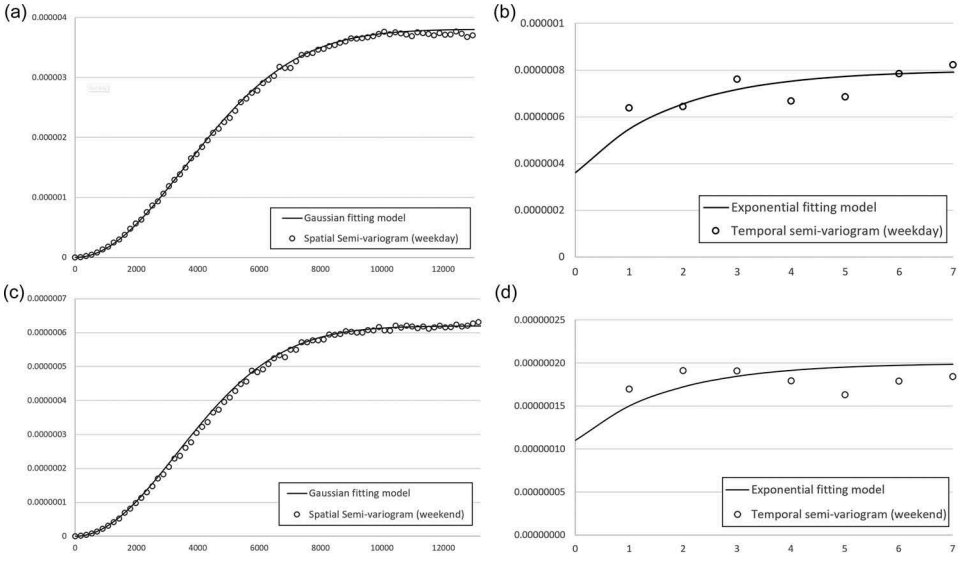

Figure 6. Spatial and temporal semi–variograms and fitting models for weekly-based periods: (a) spatial semi–variogram for weekday; (b) spatial semi–variogram for weekend; (c) temporal semi–variogram for weekday; (d) temporal semi–variogram for weekend.

well suited to the problem of fitting function selection. OLS fitted functions for the spatial and temporal semi–variograms are:

$$\gamma_s^{weekday}(h_s) = 3.81 \times 10^{-6} \cdot \left[1 - \exp\left(-\frac{h_s^2}{5042^2}\right)\right] \tag{14}$$

$$\gamma_s^{weekend}(h_s) = 0.62 \times 10^{-6} \cdot \left[1 - \exp\left(-\frac{h_s^2}{4678^2}\right)\right] \tag{15}$$

and:

$$\gamma_t^{weekday}(\mathrm{h_t}) = 0.36 \times 10^{-6} + \ 0.44 \times 10^{-6} \cdot \left[1 - \exp\left(-\frac{h_t}{1.8}\right)\right] \tag{16}$$

$$\gamma_t^{weekend}(\mathrm{h_t}) = 0.11 \times 10^{-6} + \ 0.09 \times 10^{-6} \cdot \left[1 - \exp\left(-\frac{h_t}{1.7}\right)\right] \tag{17}$$

The nugget represents a discontinuity of the semi–variogram that can be present at the origin, which is typically attributed to microscale effects or measurement errors and determine the base value of the uncertainty estimation (Kang *et al*. 2009). The value of sill is the semi–variogram's upper bound. The effective range is defined as the distance at which the semi–variance reaches 95% of the sill (Cressie 1993). Given that both temporal semi–variograms displayed a nugget effect, nuggets of temporal semi–variograms for groups of weekday and weekend were estimated from intercepts of fitting functions: 0.36×10^{-6} and 0.11×10^{-6}, respectively, as shown in Figure 6(c,d). The fitted sill values for spatial Gaussian models are 3.81×10^{-6} and

0.62×10^{-6} for weekday and weekend, respectively. The spatial effective range values are 8733 and 8102 for weekday and weekend, respectively. The fitting sill values for temporal exponential models for weekday and weekend are 0.44×10^{-6} and 0.09×10^{-6}, respectively. Temporal effective range values for weekday and weekend are 5.4 and 5.1 weeks.

Figure 7 shows the 3-D plots of the spatio-temporal covariance functions in both spatial and temporal domains for weekday (Figure 6(a)) and weekend (Figure 6(b)), respectively. The spatio-temporal covariance is a synthetic combination of the spatial covariance and temporal correlation according to Equation (11). Isotropic semi–variogram models were adopted in this study because the crime distribution tends to follow isotropic street patterns, especially in the areas near the downtown of the Cincinnati where hotspots are concentrated. We adopt the isotropic semi–variogram models because the criminal hotspots tend to distribute along all directions of the streets (Chainey *et al*. 2008, Rummens *et al*. 2017).

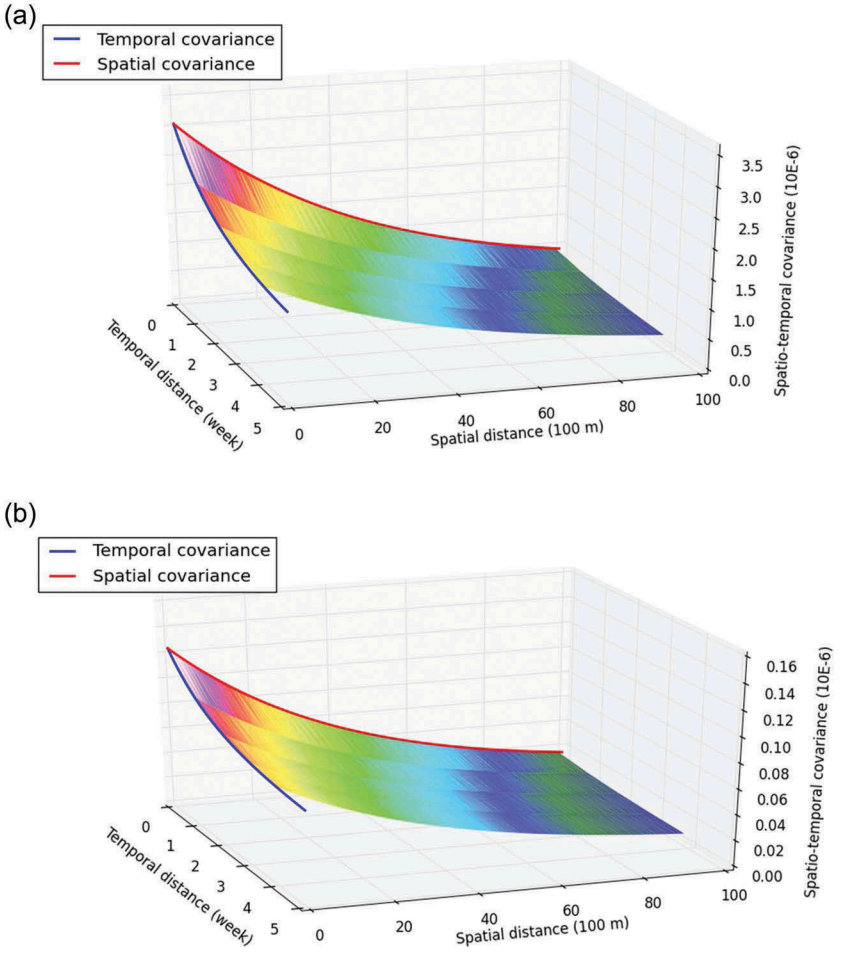

Figure 7. 3D plots of spatio-temporal covariance model for ST-Cokriging; (a) weekday; (b) weekend.

4.3. Crime prediction and validation

An iterative process was utilized, such that new crime data in the extended time series are used for the continued model calibration and validation to ensure the model is always refitted for the upcoming crime prediction. This continued calibration and validation approach helps alleviate the potential overfitting issue.

Given that July, August, and September have the largest number of street crime all over 2012 (Figure 4), last week of July, August, and September were chosen as examples to demonstrate the crime prediction results. That is, we used ST-Cokriging algorithm to predict the fourth (last) week of July, August, and September corresponding to the week 30 (started on July 23), week 35 (started on August 27), and week 39 (started on September 24) of the year 2012, and validate the crime prediction results using actual reference data.

To predict the street crime in week 30, we input the primary variable of crime risk data available in week 24–29 (6 weeks) and secondary co-variable of transitional zones. Crime data of week 30 were not used as input data, but were reserved as reference data to validate the prediction. According to the range value of the fitted covariance, the input of 6 weeks of crime data prior to the predicting time are sufficient for forecasting. This validation scenario was also applied to the crime prediction in week 35 and week 39, which crime data of week 29–34 and week 33–38 were used as source data, respectively.

Figure 8 shows the predictions of weekday street crime via the ST-Cokriging in week 30 (Figure 8(a)), 35 (Figure 8(c)), and 39 (Figure 8(e)), and the corresponding actual reference crime risk in week 30 (Figure 8(b)), 35 (Figure 8(d)), and 39 (Figure 8(f)). All figures were set to the same color scale to facilitate the comparison between the prediction results and the reference. The visual comparison shows that the predicted crime risk in Figure 8(a,c,e) closely resembles the actual reference crime risk in Figure 8(b,d,f).

Figure 9 shows the predictions of weekend street crime from the ST-Cokriging for week 30 (Figure 9(a)), 35 (Figure 9(c)), and 39 (Figure 9(e)), and the corresponding reference crime risk maps in week 30 (Figure 9(b)), 35 (Figure 9(d)), and 39 (Figure 9(f)). The high value of street crime is 0.002 (0.2%) for the crime hotspots, which is smaller than weekday due to the shorter duration. Visually, the predicted crime risk is close to the actual reference data as well.

Figure 10 shows the uncertainty estimations associated with the prediction for weekday 30 (Figure 10(a)) and weekend 30 (Figure 10(b)). The prediction uncertainty level calculated from Equation (8) is in accordance with the spatio-temporal pattern of the crime data. We used the incremental size to depict the crime data in the temporal domain. The longer temporal distance from predicting time point, the larger prediction uncertainty. Spatially, the prediction uncertainty is larger for regions lack of the crime source data.

To further validate the prediction results of ST-Cokriging, we calculated the Pearson correlation coefficient (r) and RMSE for week 30, 35, and 39 (Table 1). The correlation between predictor crime risk and reference data for weekdays in week 30, 35, and 39 is 0.7258, 0.8241, and 0.7133, respectively. The correlation for weekends in week 30, 35, and 39 is 0.6509, 0.6522, and 0.4037, respectively. The statistical correlation results indicate that the prediction achieved better results for the weekday than the weekend. Note that

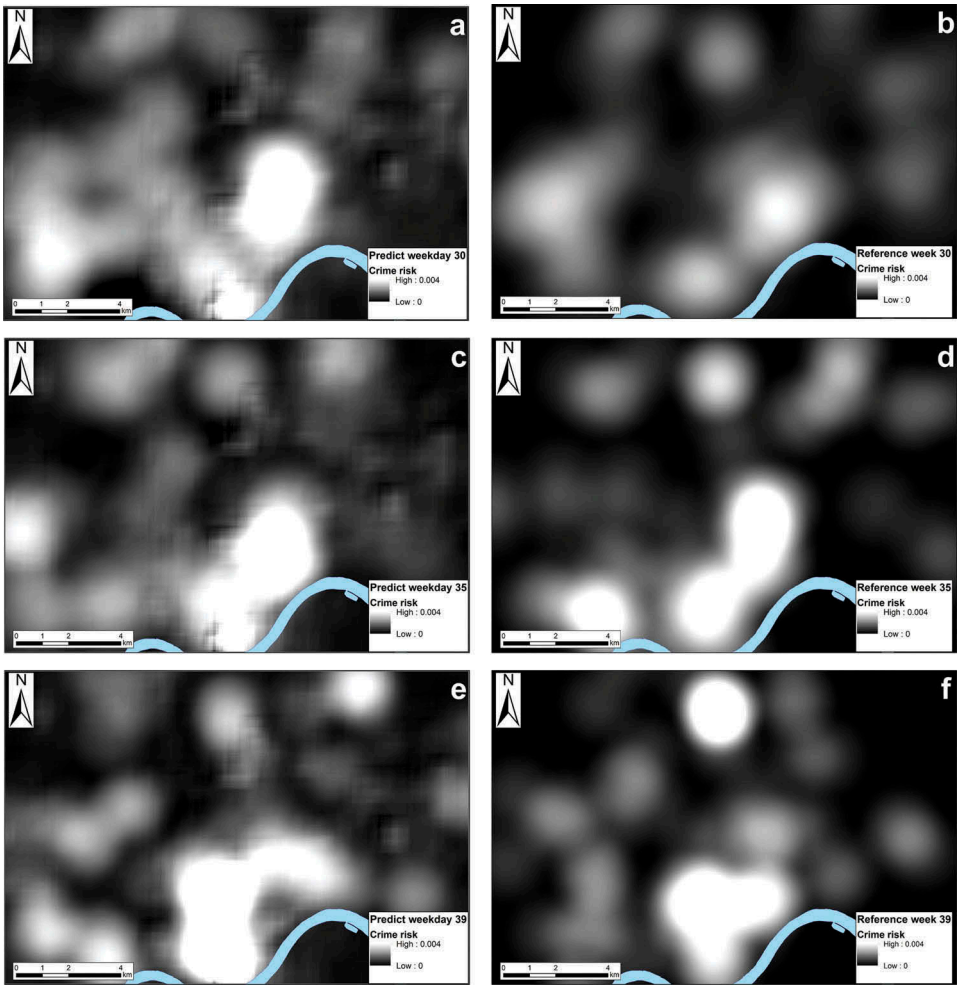

Figure 8. Weekly crime prediction results (weekday) from ST-Cokriging and validate against actual reference crime risk map: (a) ST-Cokriging prediction of week 30; (b) actual crime map of week 30; (c) ST-Cokriging prediction of week 35; (d) actual crime map of week 35; (e) ST-Cokriging prediction of week 39; (f) actual crime map of week 39.

the RMSE is smaller for weekend predictions. This is because the shorter duration of weekend leads to an overall smaller value of the crime risk.

Predictions of regular ST-Kriging without the input of co-variable were calculated with the same source of historical crime data. Statistical tests were also performed on the prediction without transitional zones as the control group (Table 1). Apparently, the use of secondary co-variable successfully increased the accuracy of crime prediction performance. Table 1 shows that in both weekday and weekend groups, the correlation of prediction increased while RMSE decreased with the support of the co-variable. Regarding the weekday groups, correlation (r) increased from 0.6923 to 0.7258 for week 30, from 0.8158 to 0.8241 for week 35, and from 0.6395 to 0.7133 for week 39 with the input of the co-variable. Regarding the weekend groups, the correlation (r) increased from 0.6286 to

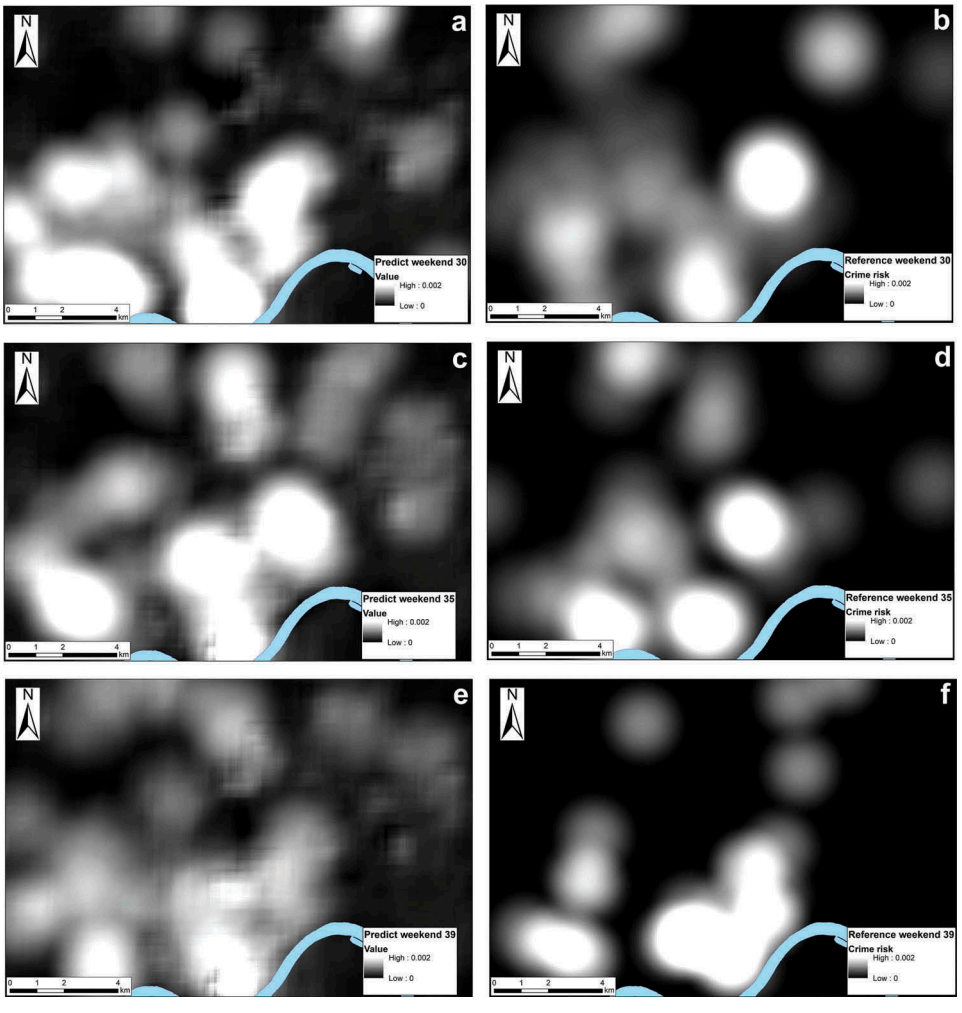

Figure 9. Weekly crime prediction results (Weekend) from ST-Cokriging and validate with actual reference crime risk map at 150 m cell size: (a) ST-Cokriging prediction of week 30; (b) actual crime map of week 30; (c) ST-Cokriging prediction of week 35; (d) actual crime map of week 35; (e) ST-Cokriging prediction of week 39; (f) actual crime map of week 39.

0.6509 for week 30, from 0.6099 to 0.6522 for week 35, and from 0.2813 to 0.4037 for week 39. All predicting results achieved positive enhancements by incorporating the transitional zones as co-variable. We calculated the average value of the correlation coefficient, the incorporation of the transitional zones as secondary co-variable increased the correlation value by 5.4% for the weekdays, as well as 12.3% for the weekends.

4.4. Crime hotspots analysis

PAI and PEI were also calculated to evaluate crime prediction accuracy. Hotspots maps were calculated by varying the threshold on the crime risk map. Afterward, hit points

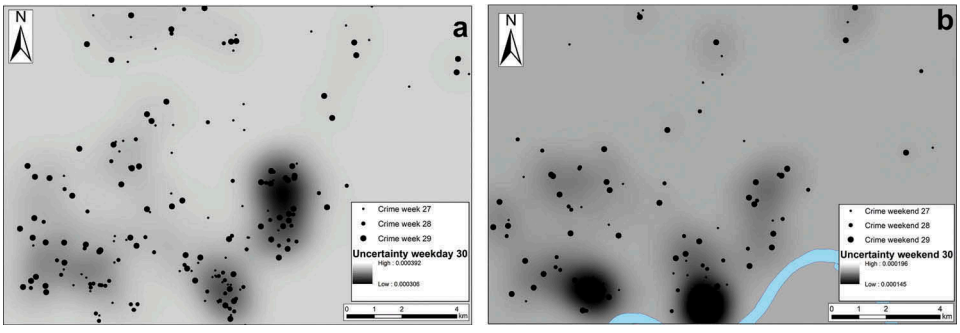

Figure 10. Uncertainty estimations associated with the prediction: (a) weekday 30; (b) weekend 30.

Table 1. Statistical tests of ST-Cokriging prediction results against reference for week-based aggregation method.

	Weekday				Weekend			
	w/ co-variable		w/o co-variable		w/ co-variable		w/o co-variable	
	r	RMSE	*r*	RMSE	*r*	RMSE	*r*	RMSE
Week 30	.7258	.001047	.6923	.003356	.6509	.000847	.6286	.002166
Week 35	.8241	.000859	.8158	.002561	.6522	.000725	.6099	.003146
Week 39	.7133	.001440	.6395	.002249	.4037	.000881	.2813	.000879

representing the captured criminal activities were obtained in the hotspots map, which were later used to calculate PAI and PEI based on Equation (12,13).

Figure 11 shows a hotspots map example generated for street crime using the threshold value of 0.0029 in weekday 30. There are three big hotspots and one small hotspot of street crime in red color. Red points are street crimes successfully predicted by the hotspots (hit points), while green points are all other street crimes. Hotspots generated from ST-Cokriging results captured clusters of street crime points very well (Figure 11). Totally, 26 out of 75 street crime points were successfully captured by the predicted hotspots for weekday 30 in 2012. The hit rate is 34.67%. Meanwhile, hotspots areas occupied 10.57% of the total study area. PAI was calculated based on Equation (12), which is 3.28 at the threshold. Then, PEI was calculated by varying threshold value, which indicates the proportion of current PAI to the maximum PAI. Regarding the case of Figure 9 with PEI value 0.7387, it is 73.87% of the maximum PAI at the crime risk threshold value of 0.0029.

We calculated the PAI curves from ST-Cokriging prediction as well as the control group without co-variable for weekdays and weekends of week 30, 35 and 39, respectively (Figure 12). PAI depicts the percentage of crime events in each week period falling into the hotspots where crimes are predicted to occur, which shows an increasing curve by varying the threshold value. Obviously, the incorporation of the secondary co-variable generates better results than the control group without the input of secondary co-variable. Note that the utilization of transitional zones enhanced the crime prediction results by complementing a significant increment of PAI values for all cases in weekday groups and weekend groups. Moreover, Table 2 shows that the PAI_{max} is higher with the use of transitional zones as the covariable than that of the control group without the covariable.

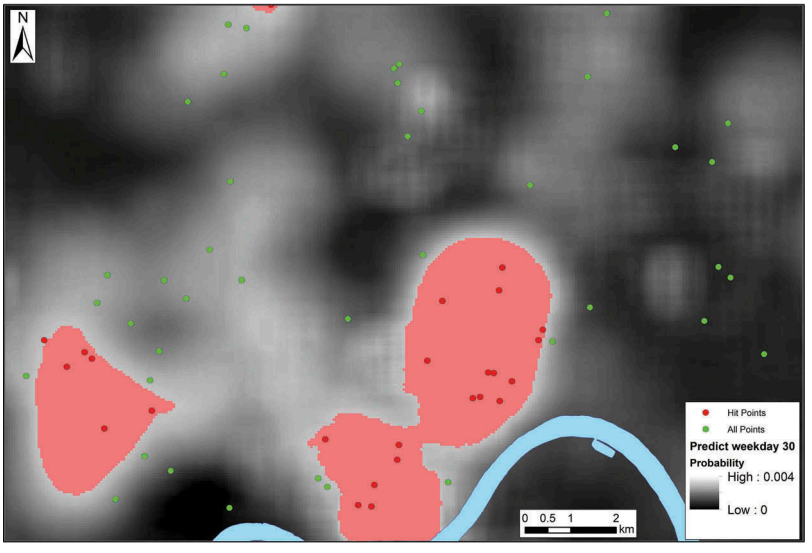

Figure 11. Predicted hotspots in weekday period 30, overlay with the actual location of street crime in weekday period 30, 2012.

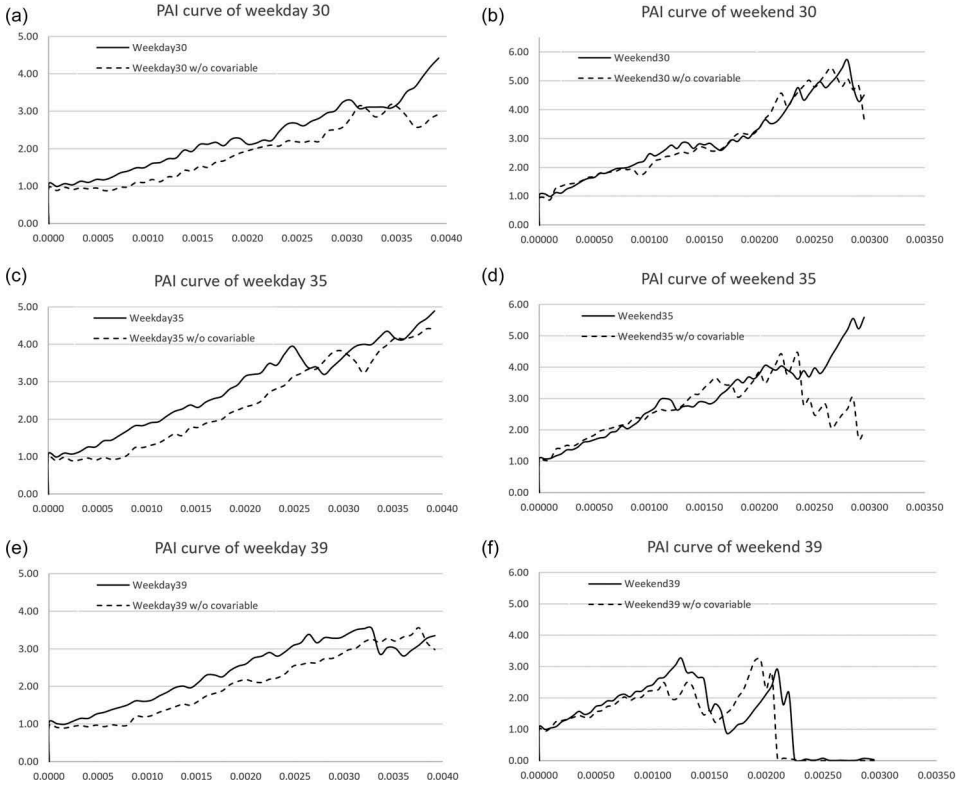

Figure 12. PAI curves of ST-Cokriging prediction result comparing with prediction without co-variable for: (a) weekday 30; (b) weekend 30; (c) weekday 35; (d) weekend 35; (e) weekday 39; (f) weekend 39.

Table 2. PAI_{max} for case group and control group for week 30, 35 and 39.

	PAI_{max} (weekday)		PAI_{max} (weekend)	
	w/ co-variable	w/o co-variable	w/ co-variable	w/o co-variable
Week 30	4.44	3.16	5.68	5.49
Week 35	4.88	4.41	5.59	4.45
Week 39	3.58	3.57	3.36	3.19

Although higher threshold value results in smaller hotspot and higher hit rate, there is a trade-off between the size of hotspots and police forces arrangement in practice. Larger hotspots captured more criminal activities, while larger hotspots size led to difficulties for the police arrangements. It is crucial to find crime hotspots in the appropriate size to efficiently arrange police forces. In this research, we chose a peak on the PAI curves as the suggested solution, which ensured an optimal PAI/PEI selection on the curve. For instance, we chose an optimal threshold value of 0.0029 for week 30 (weekday), which is corresponding to a peak of PAI valued 3.28 (Figure 9).

Following the criteria, we chose the optimal thresholds for week 30, 35, and 39 with corresponding PEI and PAI values shown in Table 3. The suggested PAI reached the highest value for weekend 30 at PAI of 5.75. The average PAI value for weekly-based results is 3.51 for weekdays and 4.36 for weekends, and the average PEI value is 0.82 for weekdays and 0.90 for weekends.

5. Discussion and conclusions

In this research, we derived and implemented a novel spatio-temporal Cokriging algorithm for predicting street crime in Cincinnati. Previous research on crime prediction research only modeled historical data (Short *et al*. 2010, Mohler *et al*. 2011, Ratcliffe *et al*. 2014, Mohler 2014), or environmental variable that correlated to criminal activities (Bendler *et al*. 2014, Gerber 2014, Patino *et al*. 2014, Corso *et al*. 2016). This study is the first attempt to predict criminal activities combining both historical crime data and an environmental variable into a rigorous spatio-temporal model. The time-series historical crime data were used as the primary variable in the ST-Cokriging algorithm, while transitional zones extracted from VIIRS nightlight imagery were used as secondary co-variable to enhance the prediction of street crime. The crime data in Cincinnati of 2012 were transformed to crime risk maps by kernel density function and then aggregated into weekly-based time-series crime maps for the prediction via the ST-Cokriging algorithm. The algorithm has been successfully applied to predict the street crime probabilities in the last week of July, August, and September (week 30, 35, and 39). The prediction results demonstrated that the algorithm generates accurate predictive crime risk maps for both weekday group and weekend group, which are close to the actual reference data in terms

Table 3. The chosen threshold and corresponding PEI for week 30, 35 and 39.

	Optimal threshold (weekday)			Optimal threshold (weekend)		
	Threshold	PEI	PAI	Threshold	PEI	PAI
Week 30	.0029	.74	3.28	.0028	.99	5.75
Week 35	.0025	.81	3.95	.0021	.71	3.97
Week 39	.0026	.92	3.31	.0012	.99	3.36

of correlation and RMSE. Also, PAI and PEI accuracy indexes were utilized in this research to evaluate the hit rate of the predicted crime hotspots. The hotspots generated from ST-Cokriging well-depicted criminal clusters in Cincinnati, which were conducive for the arrangements of the local police forces. Comparing with the prediction results using solely historical data, the transitional zones as an additional environmental variable via ST-Cokriging enhanced the crime-predicting performance in terms of higher PAI and PEI, as well as higher statistical scores.

The ST-Cokriging algorithm has been implemented to a user-friendly software tool. Because it incorporated the time-series data in the space-time domain, its computational time is longer than the traditional crime-predicting method. Efficient data structures and fast computational strategies have been incorporated into the implementation of our ST-Cokriging method. A well-known method to alleviate this difficulty is to force small covariance in the matrix to be zero, known as thresholding/tapering (Bickel *et al*. 2008). We specify this threshold based on the range value of the variograms and thus reduce the dimensionality of the covariance matrix substantially. The computation algorithms are implemented via Python language by using the mathematical and geoprocessing functions in Arcpy, Numpy, and Scipy libraries. Currently, the implemented ST-Cokriging software package can complete the calculation for the study area within 1 hour in the computer with a CPU of i7 and 16GB RAM. The algorithm presented in this research is performed and validated in Cincinnati over the year of 2012. It is also applicable in other cities for the prediction of crime risk and hotspots, providing theoretical and technical support for decision-making on police force deployment.

Acknowledgments

The authors would like to acknowledge the Cincinnati policy department for the provision of the crime data. They are also grateful to NASA Earthdata for distributing and processing the NPP-VIIRS nightlight imagery.

Disclosure statement

No potential conflict of interest was reported by the authors.

Funding

This work was supported by the University of Central Florida Preeminent Postdoctoral Program.

Notes on contributors

Dr. Bo Yang is an interdisciplinary postdoctoral researcher of GIScience at the University of Central Florida. His research interests are: GIScience, spatial statistics, machine learning algorithms, environmental and sociological modeling, UAV & drone coastal mapping.

Dr. Lin Liu is a professor of geography. His main research interests include crime analysis, urban informatics, GIS and remote sensing. He has published over 200 journal articles.

Minxuan Lan is a Ph.D. candidate at Department of Geography and GIS at the University of Cincinnati. His main research interests include crime analysis, GIS, big data and public health.

Dr. Zengli Wang is an associate professor at Nanjing Forestry University, China. His research focuses on crime prediction, crime pattern analysis and spatial data mining.

Hanlin Zhou is a master student in geography at the University of Cincinnati. His main research interests include crime research and urban informatics.

Hongjie YU is a PhD student at Sun Yat-sen University, Guangzhou, China. Her main research areas include crime geography and crime analysis.

ORCID

Bo Yang http://orcid.org/0000-0001-7439-192X
Lin Liu http://orcid.org/0000-0002-7202-3418
Minxuan Lan http://orcid.org/0000-0002-4528-9544
Zengli Wang http://orcid.org/0000-0002-1447-6689
Hanlin Zhou http://orcid.org/0000-0003-0334-5322

Data and codes availability statement

The data and codes that support the findings of this study are available in Mendeley data with the Reserved DOI: doi:10.17632/gnbk75nzxm.1 Codes are available on the Github crime-prediction repository. Crime points data with address in the folder of 'Points_Data_Private' cannot be made publicly available to protect research participant privacy and consent.

References

Ali, M. and Clausi, D., 2001. Using the Canny edge detector for feature extraction and enhancement of remote sensing images. *In: IGARSS 2001. Scanning the present and resolving the future. Proceedings. IEEE 2001 International Geoscience and Remote Sensing Symposium (Cat. No. 01CH37217)*, July, Sydney. Vol. 5. IEEE, 2298–2300.

Andresen, M.A. and Malleson, N., 2013. Crime seasonality and its variations across space. *Applied Geography*, 43, 25–35. doi:10.1016/j.apgeog.2013.06.007

Atkinson, P.M., Pardo-Igúzquiza, E., and Chica-Olmo, M., 2008. Downscaling cokriging for super-resolution mapping of continua in remotely sensed images. *IEEE Transactions on Geoscience and Remote Sensing*, 46 (2), 573–580. doi:10.1109/TGRS.2007.909952.

Baumer, E. and Wright, R., 1996. Crime seasonality and serious scholarship: a comment on farrell and pease. *British Journal of Criminology*, 36, 579. doi:10.1093/oxfordjournals.bjc.a014113

Bendler, J., *et al*., 2014. Investigating crime-to-twitter relationships in urban environments-facilitating a virtual neighborhood watch.

Bickel, P.J., Levina, E., and Levina, E.1, 2008. Regularized estimation of large covariance matrices. *Source: the Annals of Statistics the Annals of Statistics*, 36 (1), 199–227.

Binford, T.O., 1981. Inferring surfaces from images. *Artificial Intelligence*, 17 (1–3), 205–244. doi:10.1016/0004-3702(81)90025-4.

Brantingham, P. and Brantingham, P., 1995. Criminality of place crime generators and crime attractors.

Brantingham, P.J., Brantingham, P.L., and Molumby, T., 1977. Perceptions of crime in a dreadful enclosure.

Canny, J., 1986. A computational approach to edge detection. *IEEE Transactions on Pattern Analysis and Machine Intelligence*, (6), 679–698. doi:10.1109/TPAMI.1986.4767851.

Chainey, S., Tompson, L., and Uhlig, S., 2008. The utility of hotspot mapping for predicting spatial patterns of crime. *Security Journal*, 21 (1–2), 4–28. doi:10.1057/palgrave.sj.8350066.

Chan, J. and Bennett Moses, L., 2016. Is big data challenging criminology? *Theoretical Criminology*, 20 (1), 21–39. doi:10.1177/1362480615586614.

Chen, Z., *et al*., 2015. Estimating house vacancy rate in metropolitan areas using NPP-VIIRS nighttime light composite data. *IEEE Journal of Selected Topics in Applied Earth Observations and Remote Sensing*, 8 (5), 2188–2197. doi:10.1109/JSTARS.2015.2418201.

Chen, Z., *et al*., 2017. A new approach for detecting urban centers and light remote sensing. *IEEE Transactions on Geoscience and Remote Sensing*, 55 (11), 6305–6319.

Chilès, J. and Delfiner, P., 1999. Statistics for spatial data. doi:10.1046/j.1469-1809.1999.6320101.x

Corso, A., Alsudais, K., and Hilton, B., 2016. Big social data and GIS: visualize predictive crime.

Cressie, N., 1993. Statistics for spatial data: Wiley series in probability and mathematical statistics. Find this article online.

Cressie, N. and Huang, H., 1999. Classes of nonseparable, spatio-temporal stationary covariance functions. *Journal of the American Statistical Association*, 94 (448), 1330–1340. doi:10.1080/01621459.1999.10473885.

De Cesare, L., Myers, D.E., and Posa, D., 2001. Estimating and modeling space–time correlation structures. *Statistics & Probability Letters*, 51 (1), 9–14. doi:10.1016/S0167-7152(00)00131-0.

De Iaco, S., Myers, D.E., and Posa, D., 2001. Space-time analysis using a general product-sum model. *Statistics and Probability Letters*, 52 (1), 21–28. doi:10.1016/S0167-7152(00)00200-5.

Gerber, M.S., 2014. Predicting crime using Twitter and kernel density estimation. *Decision Support Systems*, 61 (1), 115–125. doi:10.1016/j.dss.2014.02.003.

Groff, E.R. and La Vigne, N.G., 2002. Forecasting the future of predictive crime mapping. *Crime Prevention Studies*, 13, 29–58.

Hall, D. and Liu, L., 2009. Cops and robbers in Cincinnati: a spatial modeling approach for examining the effects of aggressive policing. *Annals of GIS*, 15 (1), 61–71. doi:10.1080/19475680903271158.

Herbert, D.T. and Hyde, S.W., 1985. Environmental criminology: testing some area hypotheses. *Transactions of the Institute of British Geographers*, 10 (3), 259–274. doi:10.2307/622177.

Hunt, J.M., 2016. Do crime hot spots move? Exploring the effects of the modifiable areal unit problem and modifiable temporal unit problem on crime hot spot stability.

Jean, N., *et al*., 2016. Combining satellite imagery and machine learning to predict poverty. *Science*, 353 (6301), 790–794. doi:10.1126/science.aaf7894.

Kang, E.L., Liu, D., and Cressie, N., 2009. Computational statistics and data analysis statistical analysis of small-area data based on independence, spatial, non-hierarchical, and hierarchical models. *Computational Statistics and Data Analysis*, 53 (8), 3016–3032. doi:10.1016/j.csda.2008.07.033.

Kaur, B. and Garg, A., 2011. Mathematical morphological edge detection for remote sensing images. *In*: *2011 3rd international conference on electronics computer technology (ICECT)*. Kanyakumari, India: IEEE, 324–327.

Kitchin, R., 2014. Big data, new epistemologies and paradigm shifts. *Big Data & Society*, 1 (1), 2053951714528481. doi:10.1177/2053951714528481.

Law, J., Quick, M., and Chan, P., 2014. Bayesian spatio-temporal modeling for analysing local patterns of crime over time at the small-area level. *Journal of Quantitative Criminology*, 30 (1), 57–78. doi:10.1007/s10940-013-9194-1.

Levitt, S.D., 2002. Using electoral cycles in police hiring to estimate the effects of police on crime: reply. *American Economic Review*, 92 (4), 1244–1250. doi:10.1257/00028280260344777.

Li, X., *et al*., 2017. Remote sensing of night-time light, 1161 (December).

Liu, X. and Wang, M., 2016. How polycentric is urban China and why? A case study of 318 cities. *Landscape and Urban Planning*, 151, 10–20. doi:10.1016/j.landurbplan.2016.03.007

Liu, Z., *et al*., 2012. Extracting the dynamics of urban expansion in China using DMSP-OLS nighttime light data from 1992 to 2008. *Landscape and Urban Planning*, 106 (1), 62–72. doi:10.1016/j.landurbplan.2012.02.013.

Maini, R. and Aggarwal, H., 2009. Study and comparison of various image edge detection techniques. *International Journal of Image Processing (IJIP)*, 3 (1), 1–11.

Mares, D., 2013. Climate change and crime: monthly temperature and precipitation anomalies and crime rates in St. Louis, MO 1990–2009. *Crime, Law and Social Change*, 59 (2), 185–208. doi:10.1007/s10611-013-9411-8.

Mohler, G., 2014. Marked point process hotspot maps for homicide and gun crime prediction in Chicago. *International Journal of Forecasting*, 30 (3), 491–497. doi:10.1016/j.ijforecast.2014.01.004.

Mohler, G.O., *et al*., 2011. Self-exciting point process modeling of crime. *Journal of the American Statistical Association*, 106 (493), 100–108. doi:10.1198/jasa.2011.ap09546.

National, T., Estate, R., and Pike, P., 2010. An analysis of the relationship between weather and aggressive crime in Cleveland, Ohio.

Newton, A.D., Hirschfield, A., and Newton, A., 2008. Evaluation of licensing act: measuring crime and disorder in and around licensed premises.

Okabe, A., Satoh, T., and Sugihara, K., 2009. A kernel density estimation method for networks, its computational method and a GIS-based tool. *International Journal of Geographical Information Science*, 23 (1), 7–32. doi:10.1080/13658810802475491.

Pardo-Igúzquiza, E., Chica-Olmo, M., and Atkinson, P.M., 2006. Downscaling cokriging for image sharpening. *Remote Sensing of Environment*, 102 (1–2), 86–98. doi:10.1016/j.rse.2006.02.014.

Patino, J.E., *et al*., 2014. Using remote sensing to assess the relationship between crime and the urban layout. *Applied Geography*, 55, 48–60. doi:10.1016/j.apgeog.2014.08.016

Pravilovic, S., Appice, A., and Malerba, D., 2018. Leveraging correlation across space and time to interpolate geophysical data via CoKriging. *International Journal of Geographical Information Science*, 32 (1), 191–212. doi:10.1080/13658816.2017.1381338.

Proville, J., Zavala-Araiza, D., and Wagner, G., 2017. Night-time lights: A global, long term look at links to socio-economic trends. *PLoS ONE*, 12 (3), 1–12. doi:10.1371/journal.pone.0174610.

Ratcliffe, J.H., 2016. *Intelligence-led policing*. Abingdon, UK: Routledge.

Ratcliffe, J.H., Strang, S.J., and Taylor, R.B., 2014. Assessing the success factors of organized crime groups: intelligence challenges for strategic thinking. *Policing: an International Journal of Police Strategies & Management*, 37 (1), 206–227. doi:10.1108/PIJPSM-03-2012-0095.

Rodríguez-Iturbe, I. and Mejía, J.M., 1974. The design of rainfall networks in time and space. *Water Resources Research*, 10 (4), 713–728. doi:10.1029/WR010i004p00713.

Rummens, A., Hardyns, W., and Pauwels, L., 2017. The use of predictive analysis in spatiotemporal crime forecasting: building and testing a model in an urban context. *Applied Geography*, 86, 255–261. doi:10.1016/j.apgeog.2017.06.011

Sahoo, M., *et al*., 2018. Space-time cokriging approach for groundwater-level prediction with multi-attribute multiresolution satellite data. *Journal of Hydrologic Engineering*, 23, 1–7. Goovaerts 1997.

Sarkar, S. and Basu, A., 2014. Comparison of various edge detection techniques for maximum data hiding using LSB algorithm. *International Journal of Computer Science and Information Technologies*, 5 (3), 4722–4727.

Shaw, C.R. and McKay, H.D., 1942. Juvenile delinquency and urban areas.

Shi, K., *et al*., 2014. Evaluating the ability of NPP-VIIRS nighttime light data to estimate the gross domestic product and the electric power consumption of China at multiple scales: A comparison with DMSP-OLS data. *Remote Sensing*, 6 (2), 1705–1724. doi:10.3390/rs6021705.

Short, M.B., *et al*., 2010. Dissipation and displacement of hotspots in reaction-diffusion models of crime. *Proceedings of the National Academy of Sciences*, 107 (9), 3961–3965. doi:10.1073/pnas.0910921107.

Skøien, J.O. and Blöschl, G., 2007. Spatiotemporal topological kriging of runoff time series. *Water Resources Research*, 43, 9. doi:10.1029/2006WR005760

Snepvangers, J.J.J.C., Heuvelink, G.B.M., and Huisman, J.A., 2003. Soil water content interpolation using spatio-temporal kriging with external drift. *Geoderma*, 112 (3–4), 253–271. doi:10.1016/S0016-7061(02)00310-5.

Suttles, G.D., 1968. *The social order of the slum: ethnicity and territory in the inner city*. Chicago, IL: University of Chicago Press.

Sutton, P., 1997. Modeling population density with night-time satellite imagery and GIS. *Comput., Environ. And Urban Systems*, 214 (3), 227–244. doi:10.1016/S0198-9715(97)01005-3.

Uittenbogaard, A. and Ceccato, V., 2012. Space-time clusters of crime in Stockholm, Sweden. *Review of European Studies*, 4 (5), 148. doi:10.5539/res.v4n5p148.

Wang, J.F., *et al*., 2012. A review of spatial sampling. *Spatial Statistics*, 2, 1–14. doi:10.1016/j.spasta.2012.08.001

Wang, J.F., Zhang, T.L., and Fu, B.J., 2016. A measure of spatial stratified heterogeneity. *Ecological Indicators*, 67, 250–256. doi:10.1016/j.ecolind.2016.02.052

Wang, X. and Brown, D.E., 2012. The spatio-temporal modeling for criminal incidents. *Security Informatics*, 1 (1), 1–17. doi:10.1186/2190-8532-1-2.

Webster, R. and Oliver, M.A., 2007. *Geostatistics for environmental scientists*. Hoboken, NJ: John Wiley & Sons, Inc.

Welsh, B.C. and Farrington, D.P., 2002. *Crime prevention effects of closed circuit television: a systematic review*. Vol. 252. London, UK: Home Office.

Yu, B., *et al*., 2014. Object-based spatial cluster analysis of urban landscape pattern using nighttime light satellite images: a case study of China. *International Journal of Geographical Information Science*, 28 (11), 2328–2355. doi:10.1080/13658816.2014.922186.

Zhang, B. and Yang, Y., 2017. Spatiotemporal modeling and prediction of soil heavy metals based on spatiotemporal Cokriging. *Scientific Reports*, 7 (1), 1–10. Springer US. doi:10.1038/s41598-016-0028-x.

Zhao, N., *et al*., 2017. Improving accuracy of economic estimations with VIIRS DNB image products. *International Journal of Remote Sensing*, 38 (21), 5899–5918. doi:10.1080/01431161.2017.1331060.